Journal of Catalysis 269 (2010) 131–139

Contents lists available at ScienceDirect

Journal of Catalysis

journal homepage: www.elsevier.com/locate/jcat

Selective hydrogenation of chloronitrobenzene to chloroaniline in supercritical carbon dioxide over Ni/TiO_2: Significance of molecular interactions

Xiangchun Meng [a,b,c], Haiyang Cheng [b], Shin-ichiro Fujita [a], Yufen Hao [b], Yanjiao Shang [b], Yancun Yu [b], Shuxia Cai [b], Fengyu Zhao [b,*], Masahiko Arai [a,*]

[a] Division of Chemical Process Engineering, Graduate School of Engineering, Hokkaido University, Sapporo 060-8628, Japan
[b] State Key Laboratory of Electroanalytical Chemistry, Changchun Institute of Applied Chemistry, Chinese Academy of Sciences, Changchun 130022, China
[c] School of Chemical Engineering, Changchun University of Technology, Changchun 130012, China

ARTICLE INFO

Article history:
Received 25 August 2009
Revised 24 October 2009
Accepted 27 October 2009
Available online 3 December 2009

Keywords:
Chloronitrobenzene
Chloroaniline
Hydrogenation
Carbon dioxide
Intermolecular interaction

ABSTRACT

The hydrogenation of chloronitrobenzene to chloroaniline was investigated over Ni/TiO_2 at 35 °C in supercritical CO_2 ($scCO_2$), ethanol, and *n*-hexane. The reaction rate followed the order of $scCO_2$ > *n*-hexane > ethanol. In $scCO_2$, the selectivity to chloroaniline and to aniline over Ni/TiO_2 were 97–99.5% and <1%, respectively, in the conversion range of 9–100%. The high chemoselectivity to chloroaniline cannot be achieved over Ni/TiO_2 in ethanol and *n*-hexane. *In situ* high-pressure Fourier transform infrared measurements were made to study the molecular interactions of CO_2 with the following reactant and reaction intermediates: chloronitrobenzene, chloronitrosobenzene, and *N*-chlorophenylhydroxylamine. The molecular interaction modifies the reactivity of each species and accordingly the reaction rate and the selectivity. The influence of Cl substituent on the interaction modes of CO_2 with these reacting species is discussed. Possible reaction pathways for the hydrogenation of chloronitrobenzene in $scCO_2$ over Ni/TiO_2 are also proposed.

1. Introduction

The catalytic hydrogenation of chloronitrobenzene (CNB) is a common method to manufacture chloroaniline (CAN) isomers (*o*-, *m*-, and *p*-CAN), which are important intermediates in the synthesis of dyes, pharmaceuticals, and agricultural chemicals [1]. The hydrogenation of CNB, depending on the catalyst used, yields CAN through several possible pathways along with some reaction intermediates such as chloronitrosobenzene (CNSB), *N*-chlorophenylhydroxylamine (CPHA), dichloroazoxybenzene (CAOB), dichloroazobenzene (CAB), and dichlorohydrazobenzene (CHAB) (Scheme 1) [2–5]. The accumulation of these intermediates, especially CPHA, is critical when the hydrogenation of CNB is carried out in batch reactors at low or medium temperatures [3]. Because these compounds are highly toxic and problematic, their accumulation during the reaction should be avoided for the safe and green production of CAN [3–5]. To avoid the accumulation of CPHA, it is of advantage to carry out the hydrogenation at temperatures >80 °C over well-designed catalysts [4]. Chemoselective hydrogenation of aromatic nitro compounds was achieved over Au/TiO_2 and Au/Fe_2O_3 at 100–130 °C, with only trace amounts of intermediates formed [6]. The addition of small amounts of vanadium promoters could reduce the accumulation of arylhydroxylamine during the hydrogenation (120 °C) of aromatic nitro compounds over commercial Pd and Pt catalysts [3]. For Raney Ni catalysts used for the hydrogenation (30–35 °C) in organic solvents, however, the selection of effective promoters is difficult because modifiers that reduce the accumulation usually lower the reaction rate [7]. Mahata et al. communicated that when the hydrogenation of CNB was performed at 120 °C over filamentous carbon-stabilized Ni catalyst in methanol, the specific activity was ~50 mmol h^{-1} g^{-1} Ni (2.9 mmol h^{-1} $mmol^{-1}$ Ni) and there was no intermediate detected at any level of CNB conversion [8]. Their catalyst was prepared by methane decomposition over Raney Ni, which is expensive for industrial catalyst preparation. Keane and co-workers reported that selective production of CAN could be achieved in the gas-phase hydrogenation of CNB over Au/Al_2O_3 (120–250 °C), Pd-promoted Au/Al_2O_3 (Au/Pd mol/mol ⩾ 20) (120 °C), and supported Ni catalysts (120 °C) [5,9].

Dechlorination of CAN to aniline (AN) or of CNB to nitrobenzene (steps VIII, IX in Scheme 1) is another side reaction that decreases the selectivity to CAN and results in the formation of hydrogen chloride. Addition of inhibitors can minimize dechlorination, but usually lowers the reaction rate. It has recently been reported that the dechlorination process can almost completely be suppressed over several novel catalysts such as Ag/SiO_2 [10], Au/SiO_2 [11],

* Corresponding authors. Fax: +86 431 8526 2410 (F. Zhao), +81 11 706 6594 (M. Arai).
E-mail addresses: zhaofy@ciac.jl.cn (F. Zhao), marai@eng.hokudai.ac.jp (M. Arai).

0021-9517/$ - see front matter © 2009 Elsevier Inc. All rights reserved.
doi:10.1016/j.jcat.2009.10.024

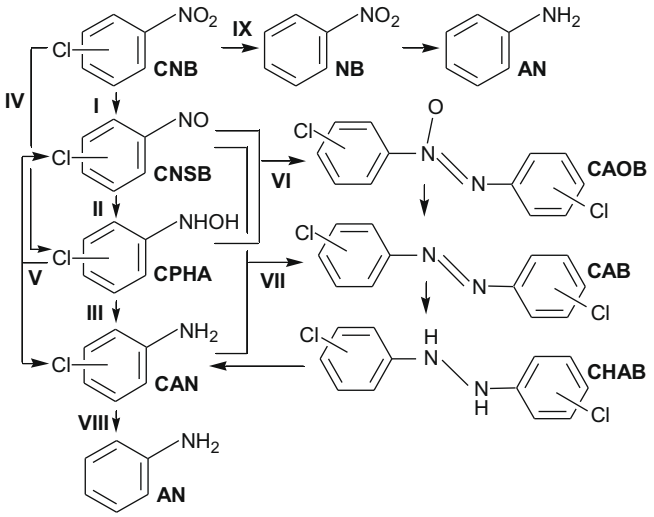

Scheme 1. Possible reaction pathways for the hydrogenation of CNB to CAN [2–5]. CNB: chloronitrobenzene, CNSB: chloronitrosobenzene, CPHA: *N*-chlorophenylhydroxylamine, CAN: chloroaniline, CAOB: dichloroazoxybenzene, CAB: dichloroazobenzene, CHAB: dichlorohydrazobenzene, AN: aniline.

Au/ZrO_2 [12], $AuPd/Al_2O_3$ [9], $Au/Fe(OH)_x$ [13], $Pt/\gamma\text{-}Fe_2O_3$ [14,15], Pt/γ-ZrP [16], decorated Pt/TiO_2 [17,18], Ru/SnO_2 [1], and Ni/TiO_2 [19]. The hydrogenation was usually carried out at 90–150 °C with Au and Ag [9–13], at 75–120 °C with Ni [8,19], and at 30–60 °C over Pt catalysts [14–18]. With these catalysts, the selectivity to the undesired AN was <1% at complete conversion of CNB. However, the use of these noble metal catalysts (Au, Ag, Pd, Ru, and Pt) in large-scale production should be practiced after a prudential consideration of the cost. Additionally, it seems necessary to improve the activity of Au and Ag catalysts for practical applications [15]. With Pt/Fe_2O_3, Pt/γ-ZrP, and Ni/TiO_2, harmful reaction intermediates such as CNSB, CPHA, CAOB, and CAB were formed in organic solvents during the reaction [14–16,19].

The melting point of *o*-, *m*-, and *p*-CNB is 32.1, 44.4, and 82 °C, respectively. To dissolve the solid CNB substrates (at room temperature), organic solvents such as methanol, ethanol, 1-butanol, hexane, cyclohexane, ethyl acetate, diethyl ether, and tetrahydrofuran are frequently used in both the liquid and the conventional gas-phase hydrogenation [1–19]. These organic solvents are volatile, toxic, and associated with serious health hazards and environmental problems. The use of traditional organic solvents is considered a major source of waste in the chemical industry. Thus, removal of the toxic solvents is significant to achieve the green production of CAN. Ionic liquid was used as a medium for the hydrogenation of *o*-CNB over ionic-liquid-like copolymer-stabilized Pt nanocatalysts, and the selectivity to CAN was >96% [20]. Because toxic organic solvents are generally used in the synthesis of ionic liquids, supercritical carbon dioxide ($scCO_2$) might be a greener alternative to conventional organic solvents. $ScCO_2$ has several merits such as non-flammability, relative inertness, complete miscibility with gases, and easy separation from liquid/solid products after reactions [21–27]. Furthermore, $scCO_2$ can show interesting effects on reaction rate and product selectivity [28–32]. Ichikawa et al. reported that the rate of hydrogenation of CNB over Pt/C was markedly enhanced and the dechlorination reaction was significantly suppressed in $scCO_2$. The selectivity to CAN was >99% at 100% conversion; however, they did not mention whether there were intermediates accumulated during the course of reaction to the complete conversion [32]. The present authors previously showed that undesired intermediates were formed and accumulated during the hydrogenation of nitrobenzene on Pt/C in $scCO_2$ [33,34]. With Pd/C, the selectivity to *o*-CAN in $scCO_2$ (92–94%) was also higher than that in ethanol (84%), but it is difficult to suppress the dechlorination reaction completely [35]. In our attempts to use supported Au catalysts such as Au/TiO_2 and Au/SiO_2 in $scCO_2$ for the CNB hydrogenation, the activity of Au catalysts was lowered monotonously with the addition of CO_2. The reduction of Au activity in dense-phase CO_2 was possibly due to the interaction of CO_2 with Au [36]. As to $Pt/\gamma\text{-}Fe_2O_3$ and $Au/Fe(OH)_x$, the acid formed *in situ* from CO_2 and a hydrogenation byproduct of H_2O are likely to impose negative effects on the support Fe_2O_3 or $Fe(OH)_x$.

Thus, it remains to be a challenging task to achieve a high chemoselectivity to CAN for the hydrogenation of CNB in green solvents over non-noble metal catalysts. Recently we have shown that the selective hydrogenation of nitrobenzene can be achieved over $Ni/\gamma\text{-}Al_2O_3$ in dense-phase CO_2 with 99% selectivity to AN over the whole conversion range of 0–100%, and molecular interactions of CO_2 with the reaction species are significant for the improvement in the selectivity [37]. The hydrogenation of CNB has a stronger tendency to give arylhydroxylamine in large amounts during the reaction [3]. Therefore, it is interesting and significant to see whether the dechlorination reaction and the accumulation of intermediates can be suppressed simultaneously during the hydrogenation of CNB with the Ni–$scCO_2$ system. The molecular interaction of CO_2 with CNB, CNSB, and CPHA is also a question of common interest because there is an electron-withdrawing substituent, –Cl, attached to the benzene ring of CNB, CNSB, and CPHA. In this work, we have studied the hydrogenation of *o*-, *m*-, and *p*-CNB over $Ni/\gamma\text{-}Al_2O_3$ and Ni/TiO_2 in $scCO_2$ at 35 °C. For comparison, the hydrogenation was also examined in ethanol and *n*-hexane under similar reaction conditions. *In situ* high-pressure Fourier transform infrared (FTIR) measurements were made to study the molecular interactions of dense-phase CO_2 with CNB, CNSB, and CPHA molecules.

2. Experimental

2.1. Catalyst preparation and characterization

Ni/TiO_2 was prepared by incipient wetness impregnation using anatase TiO_2 (specific surface area 120 $m^2\ g^{-1}$, Nanjing High Technology Nano Material Co., Ltd., China) and $Ni(NO_3)_2{\cdot}6H_2O$. Ni/Al_2O_3 was prepared by co-precipitation using $Ni(NO_3)_2{\cdot}6H_2O$ and $Al(NO_3)_3$ with a Ni/Al atomic ratio of 1/1 [37]. After drying at 120 °C, the two catalysts were calcined at 450 °C for 5 h. Before the hydrogenation run, the calcined samples were reduced under H_2 flow at 450 and 610 °C for Ni/TiO_2 and Ni/Al_2O_3, respectively.

The Ni loading in the calcined samples of Ni/Al_2O_3 and Ni/TiO_2 was measured by inductively coupled plasma optical emission spectrometry. The structural properties of Ni catalysts were examined by X-ray diffraction (XRD, Philips PW1710 BASED) and transmission electron microscopy (TEM, JEM-2000EX).

2.2. CNB hydrogenation

The hydrogenation of CNB was examined over both catalysts at 35 °C. The reaction runs in $scCO_2$ were conducted in a 50 cm^3 autoclave. The reactor was charged with CNB 1.5 g (9.52 mmol) and a catalyst sample (0.15 g Ni/TiO_2 or 0.1 g Ni/Al_2O_3), flushed with N_2, and placed into a water bath preset to 35 °C for 20 min. After the introduction of 4 MPa H_2, liquid CO_2 was introduced into the reactor with a high-pressure liquid pump (Jasco SCF-Get) to the desired pressure. The reaction was conducted while the reaction mixture was being stirred with a magnetic stirrer. After the reaction, the reactor was cooled with an ice-water bath for 20 min, depressurized carefully, and the reaction mixture was analyzed with a gas chromatograph (Shimadzu GC-2010, Rtx-5 capillary column) using a flame ionization detector. Hydrogenation reactions in ethanol

and *n*-hexane were conducted in the same reactor using similar procedures. To ensure that the amount of hydrogen in the reactor is sufficient enough for a complete conversion of CNB, all reactions were performed at an initial H_2 pressure of 4 MPa; the hydrogenation could proceed smoothly at lower H_2 pressures, as shown in our previous work [37].

2.3. Phase behavior and FTIR measurements

The solubility of CNB in $scCO_2$ in the presence of 4 MPa H_2 was measured at 35 °C by the naked eye through the transparent sapphire windows attached to an 85 cm^3 high-pressure reactor. Different amounts of CNB substrate were added into the reactor and the CO_2 pressures corresponding to phase transition were carefully determined. The details of experimental procedures were described elsewhere [31]. The phase behavior of the reactant mixture (i.e., H_2 and CNB) in dense-phase CO_2 was also examined in the same reactor; the observation was made with a similar mass/volume ratio of CNB to the reactor volume as used in the hydrogenation runs.

The high-pressure FTIR was used to examine the molecular interactions of CO_2 with the reacting species. The FTIR spectra of *p*-CNB, *p*-CNSB, and *p*-CPHA in dense-phase CO_2 were collected with the same spectrometer in similar fashions as used in the previous work [31]. The measurements were made at 35 °C and in the presence of 0–20 MPa CO_2 and 4 MPa H_2. The weight of the samples used was changed depending on its solubility in CO_2. A higher temperature of 90 °C was also used for *p*-CNB and *p*-CNSB at CO_2 pressures <4 MPa and <6 MPa, respectively. For those measurements, *p*-CNB (Wako) was used as received; commercially unavailable *p*-CNSB and *p*-CPHA, two of the intermediates (Scheme 1), were synthesized by the oxidation of *p*-CAN (Wako) with H_2O_2 catalyzed with ammonium molybdate [38], and by the reduction of *p*-CNB with zinc dust [39], respectively. The formation of these compounds was confirmed by FTIR and NMR (JEOL A200II) [38,40].

3. Results and discussion

3.1. Properties of Ni catalysts

Ni/Al_2O_3 was the same as used previously for the hydrogenation of nitrobenzene; the average Ni particle size was ca. 8.5 nm [37]. The Ni loading of Ni/Al_2O_3 and Ni/TiO_2 was 41% and 16%, respectively. The XRD patterns and TEM images of Ni/TiO_2 are presented in Fig. 1. After calcination, the existence of NiO and anatase TiO_2 was identified. After reduction, Ni particles in size mostly between 5 and 25 nm were formed. The average particle size determined from the XRD line broadening was ca. 14 nm.

3.2. Features of Ni catalysts for selective hydrogenation of CNB

Table 1 shows the results of *o*-CNB hydrogenation over Ni/Al_2O_3 and Ni/TiO_2 in $scCO_2$ at 35 °C. The selectivity to the desired *o*-CAN at ca. 80% conversion was >98% and 99% over Ni/Al_2O_3 and Ni/TiO_2, respectively. Moreover, the turnover frequency (TOF) value for the reaction over Ni/Al_2O_3 was much less than that over Ni/TiO_2 (entries 1 and 2). These results indicate that chemoselective hydrogenation of *o*-CNB can be achieved in $scCO_2$ over both Ni catalysts, especially over Ni/TiO_2.

Table 1 also compares the results of *o*-CNB hydrogenation over Ni/TiO_2 in $scCO_2$ with that in polar ethanol and apolar *n*-hexane at 35 °C. The rate of *o*-CNB conversion was the highest in $scCO_2$ and the lowest in ethanol. The TOF value in $scCO_2$ was ~3.1 and ~1.4 times higher than that in ethanol and *n*-hexane, respectively. In ethanol, the dechlorination reaction was negligible but the intermediates including CNSB, CAOB, CAB, and CHAB were formed in a significant amount (entries 3, 4). Because CPHA decomposes to CNSB and CAN during gas chromatograph analysis [42], the formation of CPHA during the hydrogenation cannot be excluded. Chen and co-workers, who performed the hydrogenation of CNB at 90 °C over Ni/TiO_2 in ethanol, also observed the formation of significant amounts of intermediates and negligible amount of AN [19]. In contrast, there was no accumulation of intermediates in *n*-hexane, but a slight dechlorination occurred (entry 5). In $scCO_2$, both the dechlorination and the accumulation of intermediates were suppressed satisfactorily; the selectivity to *o*-CAN was 99% at 82% conversion (entry 2).

Fig. 2 shows the evolution of product species with time during the hydrogenation of *o*-CNB over Ni/TiO_2 in $scCO_2$. The yield of *o*-CAN is similar to the conversion of *o*-CNB over the whole conversion range from 9% to ~100%; the yield of all byproducts including AN and reaction intermediates decreased from <3.5% in 5 min to <1% after 30 min. Thus, Ni/TiO_2 is very effective for the chemoselective hydrogenation of *o*-CNB in $scCO_2$. The combination of $scCO_2$ and Ni/TiO_2 is also effective for the chemoselective hydrogenation of *m*- and *p*-CNB isomers (Table 2).

The suppression of formation of hydroxylamine is a topic of industrial importance because aryl hydroxylamines are generally accumulated in large amounts during the hydrogenation of nitroaromatics with electron-withdrawing substituents (e.g., halogen and sulfonamide) [3,7]. Studer et al. found that the accumulation of hydroxylamine in methanol at 30–35 °C could be reduced from 70%–80% over unmodified Raney Ni to 11% by careful selection of vanadium promoters; simultaneously, the reaction rate was down by a factor of 0.1 [7]. Mahata et al. communicated that there was no intermediate detected in methanol during the hydrogenation of *o*- and *p*-CNB over filamentous carbon-stabilized Ni catalyst,

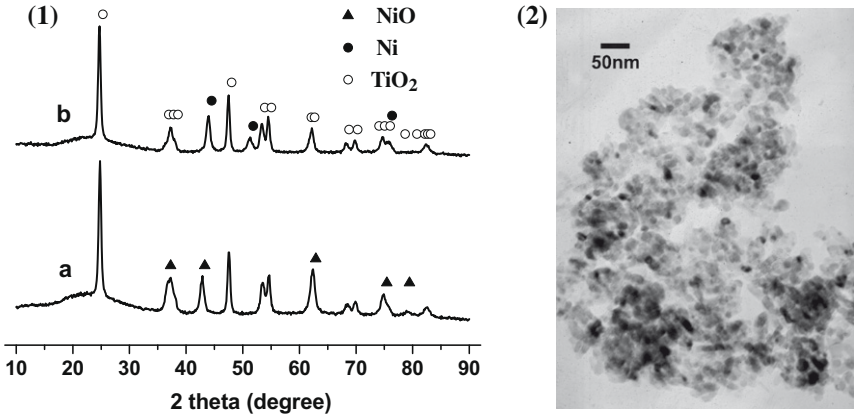

Fig. 1. (1) XRD patterns of Ni/TiO_2: (a) calcined under air at 450 °C, (b) reduced with H_2 at 450 °C; (2) TEM image of Ni/TiO_2 after reduction with H_2 at 450 °C.

Table 1
Hydrogenation of *o*-CNB over 41 wt% Ni/Al_2O_3 in $scCO_2$ and over 16 wt% Ni/TiO_2 in different reaction media.

Entry	Medium	Catalyst	C_0[a] ($mmol\ cm^{-3}$)	Conv. (%)	Selectivity (%)			TOF[b] (h^{-1})
					o-CAN	AN	Others	
1	$scCO_2$	Ni/Al_2O_3	0.19	78[c]	>98	<1.5	<0.5	90
2	$scCO_2$	Ni/TiO_2	0.19	82	99	<1	<1	318
3	Ethanol[d]	Ni/TiO_2	0.19	26	70	<1	>29[e]	101
4	Ethanol	Ni/TiO_2	0.95	36	70	–[f]	30[e]	140
5	*n*-Hexane	Ni/TiO_2	0.95	59	97	2	1	229

Reaction conditions: H_2 4 MPa, *o*-CNB 1.5 g (9.52 mmol), Ni/Al_2O_3 0.1 g or Ni/TiO_2 0.15 g, organic solvent 10 cm^3 or CO_2 10.5 MPa, reactor 50 cm^3, 35 °C, 50 min.
[a] Initial concentration of *o*-CNB.
[b] Turnover frequency of hydrogenation of *o*-CNB. The number of active sites was calculated using the average nickel diameter (d) determined by XRD line broadening *via* the following equation: Dispersion = $6(v_m/a_m)/d$, where v_m and a_m are equal to 10.95 $Å^3$ and 6.51 $Å^2$, respectively, for Ni [41].
[c] After 60 min of reaction.
[d] Ethanol 50 cm^3, reactor 100 cm^3.
[e] Other products in ethanol include CNSB, CAOB, CAB, and CHAB.
[f] Not detected.

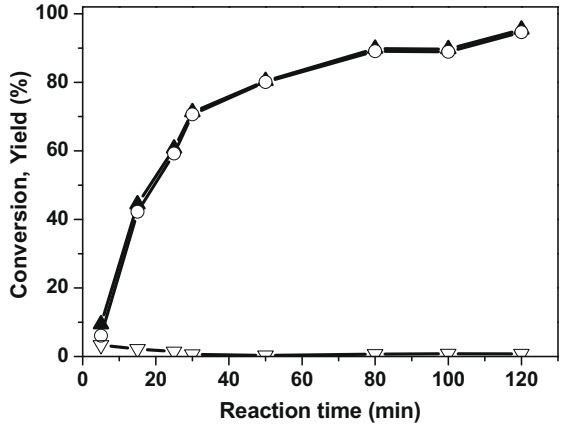

Fig. 2. Evolution of species with time during the hydrogenation of *o*-CNB over 16 wt% Ni/TiO_2 in $scCO_2$ at 35 °C. Reaction conditions: Ni/TiO_2 0.15 g, CO_2 11 MPa. (▲) *o*-CNB conversion, (○) *o*-CAN yield, (▽) total yield of all byproducts.

and the specific activity was ~50 $mmol\ h^{-1}\ g^{-1}$ Ni (2.9 $mmol\ h^{-1}\ mmol^{-1}$ Ni) at 120 °C under 1.5 MPa H_2 [8]. Recently, we have shown that the accumulation of intermediates during the hydrogenation of nitrobenzene can be completely avoided over Ni/Al_2O_3 in dense-phase CO_2 [37]. The present hydrogenation of *o*-CNB over Ni/TiO_2 in $scCO_2$ gave a TOF value of 318 h^{-1} (22.9 $mmol\ h^{-1}\ mmol^{-1}$ Ni) at 35 °C under an initial H_2 pressure of 4 MPa; the TOF value was much higher than that in ethanol and *n*-hexane (Table 1). Additionally, it is difficult to achieve a high chemoselectivity in both ethanol and *n*-hexane because either significant accumulation of intermediates or slight dechlorination takes place. In the context, the present results are important because the reduction of intermediates can be achieved along with the increased reaction rate and the negligible dechlorination. In other words, the effectiveness of $scCO_2$ and Ni catalysts for the reduction of intermediates can be extended to a more challenging task of chemoselective hydrogenation of CNB in the absence of organic solvents. To our knowledge, such a chemoselective hydrogenation of CNB to CAN over Ni catalysts at mild temperature has not been reported so far.

3.3. Influence of CO_2 pressure and phase behavior

The present hydrogenation occurs in a multi-phase system, in which the reaction rate and/or the product distribution may depend on the phase behavior. The hydrogenation of CNB was studied with the most effective Ni/TiO_2 catalyst at different CO_2 pressures while making the other conditions unchanged. Before the reaction results, the phase behavior observations are given first. Fig. 3 shows the changes in the phase state of CNB isomers in $scCO_2$ at different CO_2 pressures and at 35 °C in the presence of 4 MPa H_2. At 35 °C, *m*- and *p*-CNB are solid in the absence of CO_2; *m*-CNB turned into liquid at ca. 3.6 MPa CO_2 indicating that its melting point could be lowered to <35 °C under dense-phase CO_2. The CNB substrates were soluble to some extent in $scCO_2$ at 35 °C and their quantities in $scCO_2$ increased with CO_2 pressure. The solubility was influenced somewhat by the substituent position of the CNB isomers and followed the order of *m*- > *o*- and *p*-CNB. With the same ratio of CNB weight to reactor volume as used in the hydrogenation runs, the phase transition from two phases to a single phase occurred at CO_2 pressures of 12.3, 10.2, and 12.8 MPa for *o*-, *m*-, and *p*-CNB, respectively. Upon careful depressurization, the reverse transition was observed at 11.8, 9.6, and 11.6 MPa for *o*-, *m*-, and *p*-CNB, respectively.

The influence of CO_2 pressure was examined with a selected substrate of *o*-CNB. Fig. 4 shows the changes in the conversion of *o*-CNB and the selectivity to *o*-CAN with CO_2 pressure. The total conversion of *o*-CNB increased first and then decreased with increasing CO_2 pressure. The conversion was maximal at ca. 9–12.5 MPa CO_2. The pressure for the maximum conversion is close

Table 2
Results of hydrogenation of *m*- and *p*-CNB in $scCO_2$ over 16 wt% Ni/TiO_2.

Entry	Reactant	CO_2 (MPa)	Time (min)	Conv. (%)	Selectivity (%)		
					CAN	AN	Others
1	*m*-CNB	11	30	64	96	<0.1	4
2			80	100	>99.5	<0.5	<0.1
3	*p*-CNB	10	30	51	99	–[a]	1
4			90	100	>97	<0.5	<2.5

Reaction conditions: CNB 1.5 g (9.52 mmol), H_2 4 MPa, 16 wt% Ni/TiO_2 0.15 g, 35 °C.
[a] Not detected.

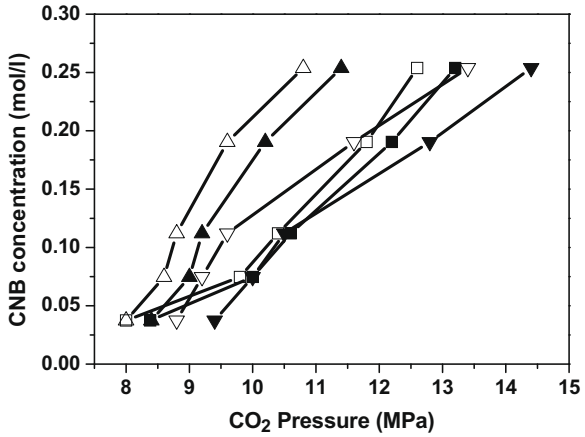

Fig. 3. The phase behavior of *o*- (■, □), *m*- (▲, △), and *p*-CNB (▼, ▽) in CO_2 at 35 °C in the presence of 4 MPa H_2. A certain amount of *o*-CNB was added to the view cell, H_2 was introduced up to 4 MPa, and then CO_2 was gradually introduced until the liquid *o*-CNB disappeared at a CO_2 pressure P_1. Upon carefully depressurization, the first liquid drop of *o*-CNB appeared at a pressure P_2. These two pressures P_1 and P_2 were carefully determined at several amounts (concentrations in the cell) of *o*-CNB, and are given with solid and open marks, respectively. The data for *m*- and *p*-CNB were collected using the same procedures.

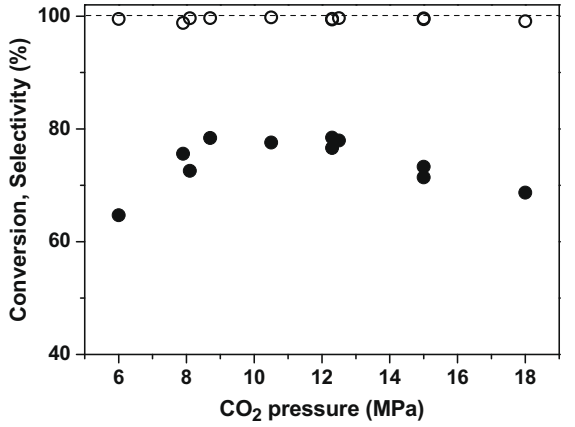

Fig. 4. Influence of CO_2 pressure on the conversion of *o*-CNB (●) and the selectivity to *o*-CAN (○) in the hydrogenation of *o*-CNB over 16 wt% Ni/TiO_2 at 35 °C and at H_2 4 MPa for 50 min.

to that of the reversible phase transition of *o*-CNB (11.8–12.3 MPa CO_2), indicating that the phase behavior is an important factor in determining the rate of CNB hydrogenation. However, the high selectivity to *o*-CAN remained unchanged when the reaction mixture changed from the gas–liquid–solid system to the gas–solid system.

3.4. FTIR measurements: molecular interactions with CO_2

High-pressure FTIR was used to examine molecular interactions of dense-phase CO_2 with such selected reacting species as *p*-CNB, *p*-CNSB, and *p*-CPHA, which would affect the reaction pathways of selective hydrogenation of CNB and change the reaction rate and the product selectivity.

3.4.1. p-CNB

Fig. 5 shows the FTIR spectra of nitro group vibrations in the presence of 4 MPa H_2 and 0–20 MPa CO_2. The result of *p*-CNB in ethanol is also shown for comparison. The bands at ca. 1343 and 1521 cm^{-1} were assigned to the symmetric and asymmetric

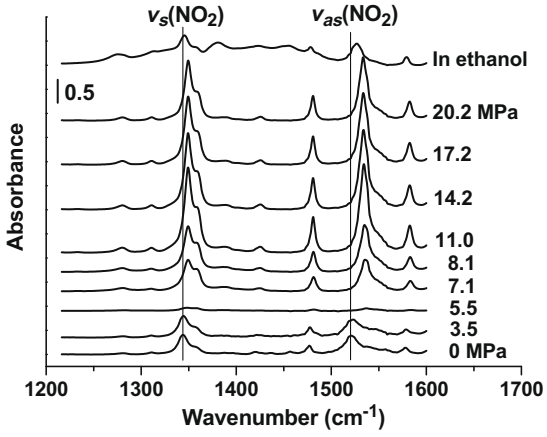

Fig. 5. FTIR spectra of nitro group stretching vibrations for *p*-CNB in the presence of 4 MPa H_2 and dense-phase CO_2 at different pressures given. The spectra at CO_2 pressures <4 MPa and >5 MPa were collected at 90 °C and 35 °C, respectively. Also included are the same group vibrations of *p*-CNB in ethanol (*p*-CNB/ethanol = 0.05, molar ratio) at room temperature.

stretching vibrations of the nitro group, $\nu_s(NO_2)$ and $\nu_{as}(NO_2)$ [2]. The peaks of $\nu_s(NO_2)$ and $\nu_{as}(NO_2)$ were shifted with CO_2 pressure, and these shifts are depicted in Fig. 6. The peak position of $\nu_s(NO_2)$ was blue shifted from 1343 cm^{-1} at 0 MPa CO_2 to 1350 cm^{-1} at 7 MPa CO_2 and remained unchanged at 7–20 MPa CO_2. The peak position of $\nu_{as}(NO_2)$ was also blue shifted from 1521 to 1538 cm^{-1} with CO_2 pressure up to ca. 5.5 MPa; between 5.5 and 20 MPa CO_2, the peak position was slightly shifted to a lower wavenumber and then changed little. The absorption bands at 20 MPa CO_2 were located at larger wavenumbers than those at 0 MPa CO_2 and in ethanol. These FTIR results indicate that the N–O bond of the nitro group becomes stronger in the presence of dense-phase CO_2 compared to the ambient gas and liquid conditions. Additionally, it was observed that an absorption band appeared at 1109 cm^{-1} at 0 MPa CO_2 and was blue shifted to 1112 cm^{-1} with CO_2 pressure up to 7 MPa, above which it did not change further (not shown). This band is due to the C–N stretch [43].

The above changes of $\nu_s(NO_2)$ and $\nu_{as}(NO_2)$ for *p*-CNB with CO_2 pressures were similar to those of nitrobenzene in dense-phase CO_2 [37]. We have proposed that the overall IR result of nitrobenzene in dense-phase CO_2 is controlled by the following modes of interactions between CO_2 molecules and the nitro group: (1) one

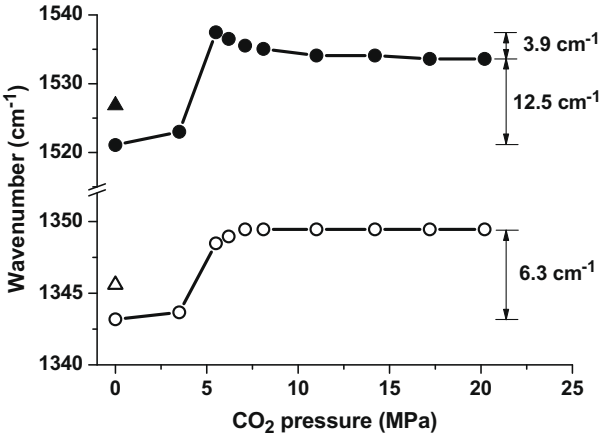

Fig. 6. Influence of CO_2 pressure on the absorption peak position of $\nu_s(NO_2)$ and $\nu_{as}(NO_2)$ of *p*-CNB. (○) Symmetric and (●) asymmetric stretching vibrations in dense-phase CO_2; (△) symmetric and (▲) asymmetric stretch in ethanol (*p*-CNB/ethanol = 0.05, molar ratio) at room temperature.

of the oxygen atoms of CO_2 interacts with the positive nitrogen of $-NO_2$ group and (2) the carbon atom of CO_2 interacts with the oxygen of $-NO_2$ group. The former interaction might strengthen both the C–N and N–O bonds, while the latter might weaken the strength of the N–O bond. The former interaction has a dominant effect on the stretch vibration of N–O bond [37]. It seems likely that the nitro group of *p*-CNB interacts with CO_2 in the same modes as in the case of nitrobenzene.

At similar CO_2 pressures, the bands of $\nu_s(NO_2)$ and $\nu_{as}(NO_2)$ of *p*-CNB appeared at lower wavenumbers than those of the corresponding peaks of nitrobenzene. For example, the wavenumbers of $\nu_s(NO_2)$ and $\nu_{as}(NO_2)$ for *p*-CNB at 20 MPa CO_2 were 1350 and 1534 cm^{-1}; the corresponding values for nitrobenzene were 1354 and 1538 cm^{-1}, respectively [37]. The difference in wavenumbers of the nitro group vibrations between *p*-CNB and nitrobenzene might be due to the Cl substituent, an electron-withdrawing group attached to the benzene ring of *p*-CNB.

3.4.2. p-CNSB

Fig. 7 shows the FTIR spectra of the nitroso (N=O) moiety of *p*-CNSB in the presence of 4 MPa H_2 and 0–20 MPa CO_2. The spectrum of *p*-CNSB in ethanol at room temperature was recorded for comparison. The absorption bands at 1109 and 1517 cm^{-1} before the introduction of CO_2 are due to the C–N stretch of the CNSB monomer and the stretching vibration of N=O, respectively [43]. The peak position of ν(C–N) of CNSB monomer was slightly blue shifted from 1109 to 1116 cm^{-1} with the increase of CO_2 pressure up to ca. 15 MPa and then remained unchanged. We have shown that the N=O group of nitrosobenzene can interact with CO_2 molecules through its oxygen (O-interacted) and nitrogen (N-interacted) atoms; the stretching vibration of N=O gives a band around 1520 cm^{-1} in the former case and a band at 1485 cm^{-1} in the latter case [37]. Thus, the band at ca. 1510 cm^{-1} in the spectra of *p*-CNSB would arise from the stretching vibration ν(N=O)(O-interacted). The peak position of ν(N=O)(O-interacted) changed with CO_2 pressure and these shifts are shown in Fig. 8. The stretching vibration ν(N=O)(O-interacted) in CO_2 was monotonously red shifted with CO_2 pressure up to 13 MPa and then remained unchanged. Additionally, there was no peak at 1485 cm^{-1} in the spectra of *p*-CNSB at all pressures examined. Therefore, the N=O of *p*-CNSB interacts with the carbon of CO_2 through its oxygen but not through its nitrogen. The N=O group functions as a Lewis base (LB) and CO_2 plays a role of a Lewis acid (LA). This type of intermolecular interaction becomes stronger with the increase in CO_2 pressure and weakens the N=O bond of *p*-CNSB. Simultaneously, the C–N stretch band was blue shifted, in agreement with the previous results for nitroso compounds that ν(C–N) increases when ν(N=O) decreases [37,43].

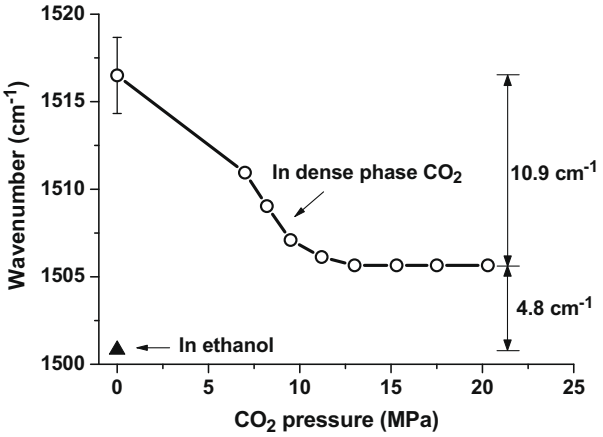

Fig. 8. Influence of CO_2 pressure on the peak position of the nitroso group (O-interacted) vibration for *p*-CNSB at 35 °C. The spectrum in the absence of CO_2 (0 MPa) was collected at 90 °C. Also shown is the same group vibration in ethanol (*p*-CNSB/ethanol = 0.03, molar ratio) at room temperature.

At 20 MPa CO_2, the peak position of ν(N=O)(O-interacted) was at 1506 cm^{-1}, which was still higher than that in ethanol (1501 cm^{-1}). This difference is similar to that of nitrosobenzene, indicating that the LA–LB interaction of CO_2 with the N=O group of *p*-CNSB is also less strong compared with the hydrogen bonding in ethanol [37].

In the spectra of *p*-CNSB, the band of ν(N=O)(O-interacted) was shifted from 1517 cm^{-1} at 0 MPa CO_2 to 1506 cm^{-1} at 20 MPa CO_2; in the case of nitrosobenzene, the same vibration gave a band at 1521 and 1513 cm^{-1} at the corresponding pressures [37]. That is, the stretching vibration of N=O of *p*-CNSB is less strong than that on nitrosobenzene at similar CO_2 pressures. The difference might be due to the electron-withdrawing effect of the Cl substituent of *p*-CNSB.

3.4.3. p-CPHA

The FTIR spectra of *p*-CPHA in dense-phase CO_2 and in ethanol are given in Fig. 9. The absorption bands at ca. 920, 1494–1500,

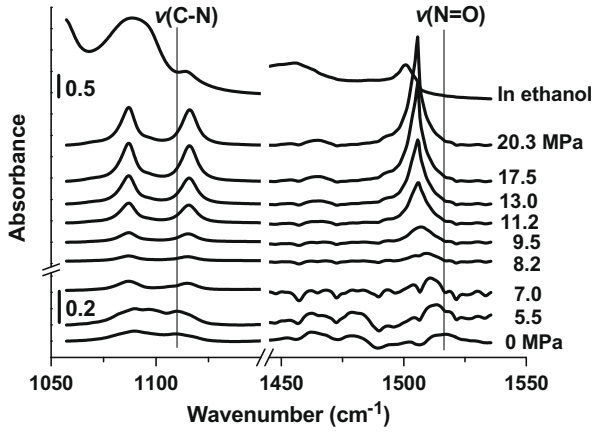

Fig. 7. FTIR spectra of *p*-CNSB in the presence of 4 MPa H_2 and dense-phase CO_2 at pressures given. The spectra at CO_2 pressures <6 MPa and >6 MPa were collected at 90 °C and 35 °C, respectively. Also shown is the spectrum of *p*-CNSB in ethanol (*p*-CNSB/ethanol = 0.03, molar ratio) at room temperature.

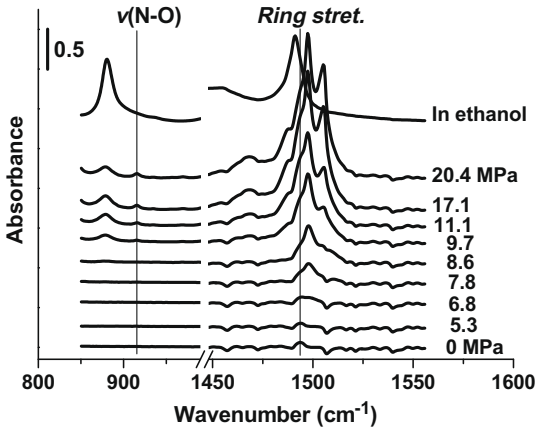

Fig. 9. FTIR spectra for the ring stretching vibration of *p*-CPHA in the presence of 4 MPa H_2 and dense-phase CO_2 at pressures given (35 °C). The spectrum of *p*-CPHA in ethanol (*p*-CPHA/ethanol = 0.15, molar ratio) collected at room temperature is also shown.

and 3200 cm^{-1} are related to the N–O stretch, a ring stretching mode, and the O–H stretching vibration of phenylhydroxylamine derivatives, respectively [44,45]. The O–H stretch band of *p*-CPHA in dense-phase CO_2 was not distinct at all pressures examined, possibly because $scCO_2$ has a combination band in the region where the stretching vibration of O–H occurs [46]. The N–O stretch of *p*-CPHA could only be identified at 915 cm^{-1} above 8 MPa CO_2, and its peak position did not show any shift with CO_2 pressures from 8 to 20 MPa. Here, our interest is focused on the absorption band at 1494 cm^{-1}, which is related to the ring stretch of *p*-CPHA, for the discussion on interactions between *p*-CPHA and CO_2 molecules.

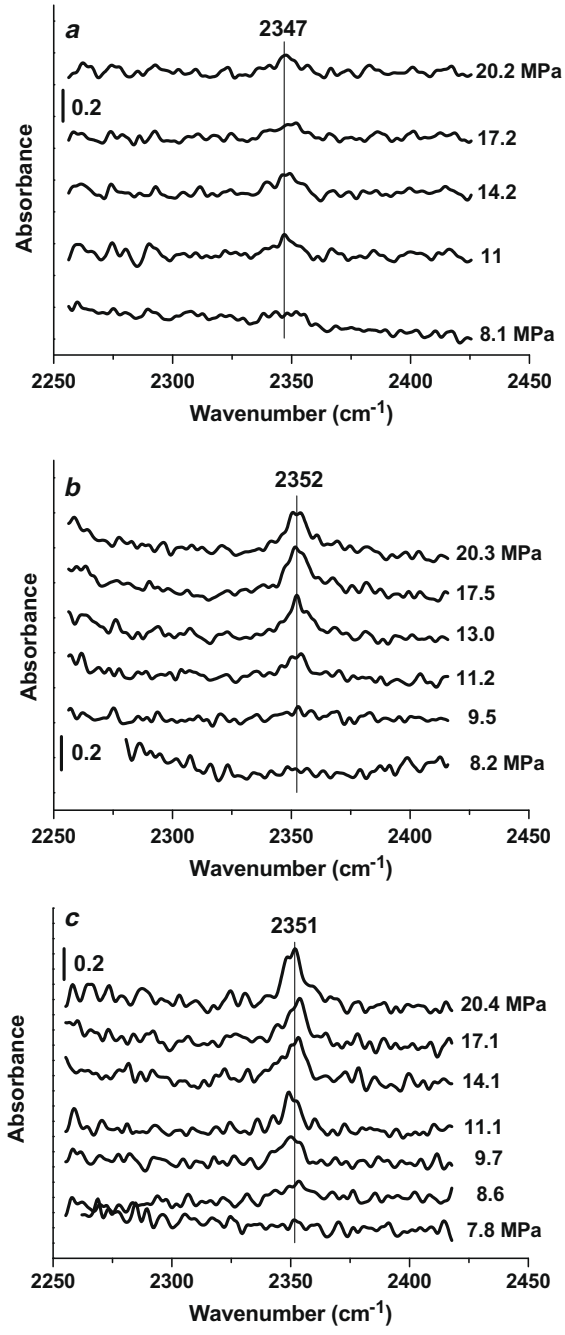

Fig. 10. FTIR difference spectra in the CO_2 v_3-antisymmetric-stretching mode region for the CO_2-*p*-CNB (a), CO_2-*p*-CNSB (b), and CO_2-CPHA (c) system at CO_2 pressures given. All spectra were collected at 35 °C in the presence of 4 MPa H_2. The difference spectra were obtained by using the substrate-absent system at the corresponding pressures as background.

The position of the ring absorption band at 1494 cm^{-1} scarcely changed between ca. 0 and 5 MPa CO_2, and was blue shifted to 1498 cm^{-1} with further increasing CO_2 pressure up to ca. 8 MPa. At 9.7–20.4 MPa CO_2, the band split into two peaks at 1498 and 1505 cm^{-1}, and their positions did not change with CO_2 pressures. The splitting of the ring absorption band was also observed for *N*-phenylhydroxylamine at above 8 MPa CO_2; however, the band was red shifted at 4–11 MPa CO_2 and its position remained unchanged from 11 to 20 MPa CO_2 [37].

3.4.4. CO_2

Interactions of CO_2 with LB, polymer, or ionic liquids cause some changes in the IR spectra corresponding to the CO_2 v_2-bending (610–680 cm^{-1}) and v_3-antisymmetric stretching (2100–2500 cm^{-1}) mode regions [47–49]. It was impossible to distinguish the v_2 mode in our IR results. Fig. 10 gives the FTIR spectra of CO_2 in the v_3 region for the CO_2–*p*-CNB, CO_2–*p*-CNSB, and CO_2–*p*-CPHA systems at different CO_2 pressures. The results in Fig. 10 were obtained by using the substrate-absent system at the corresponding pressures as background. For the CO_2–*p*-CNB system, there was one main peak at 2347 cm^{-1} at CO_2 pressures >8 MPa and the peak position scarcely changed with CO_2 pressure. For the CO_2–*p*-CNSB system, there was only one peak at 2352 cm^{-1} at above 9.5 MPa, and its position did not change with CO_2 pressure. The fact that only one band appears in the v_3 region suggests that there is only one type of the site within the *p*-CNB or *p*-CNSB molecule to interact with CO_2 molecules [48]. Additionally, the wavenumber of the C=O stretching vibration of CO_2 in the CO_2–*p*-CNB system was lower than that in the CO_2–*p*-CNSB system. This indicates that the C=O bond strength of CO_2 is weaker in the CO_2–*p*-CNB system than that in the CO_2–*p*-CNSB system. The IR results of *p*-CNB have shown that the interaction of CO_2 through its oxygen with the nitrogen of $–NO_2$ group had a dominant effect on the stretching vibration of N–O bond; both the C–N and N–O bonds were strengthened. It seems likely that the interaction between CO_2 and *p*-CNB induces partial electron transfer from the C=O bond of CO_2 to the C–N and N–O bonds of *p*-CNB, and this weakens the C=O bond of CO_2. In contrast, the N=O of *p*-CNSB interacted with the carbon of CO_2 through its oxygen (not nitrogen), and the N=O bond was weakened with CO_2 pressures. The interaction of CO_2 with *p*-CNSB is likely to induce partial electron transfer from the N=O bond of *p*-CNSB to the C=O bond of CO_2, strengthening the C=O bond. Thus, the IR spectra of CO_2 provide additional evidence for the interaction mode of CO_2 with *p*-CNB and *p*-CNSB.

Fig. 10c shows the FTIR difference spectra of CO_2 in the v_3 region for the CO_2–*p*-CPHA system at different pressures. At above 8.6 MPa CO_2, there was one or two peaks at around 2351 cm^{-1} with no other peaks in the v_3 region. In contrast, an additional peak appears at 2332 cm^{-1}along with the bands at 2348–2355 cm^{-1} for the CO_2–*N*-phenylhydroxylamine system [37]. This indicates that *p*-CPHA does interact with CO_2; however, the available sites within the *p*-CPHA molecule for CO_2 are less than those within the *N*-phenylhydroxylamine molecule. Presumably, CO_2 interacts with *p*-CPHA through its carbon.

3.5. Improvement of the selectivity to CAN

The dechlorination reaction was suppressed over Ni/TiO_2 in either ethanol or $scCO_2$, which might be mainly related to the properties of Ni/TiO_2. The formation of harmful intermediates occurring in ethanol was almost completely retarded in $scCO_2$, indicating the significance of medium effects. The FTIR results show that the strength of the N–O bond of CNB in dense-phase CO_2 was stronger than that in the ambient gas phase and it increased with CO_2 pressure up to ca. 6 MPa, above which it slightly decreased (Fig. 6). However, the strength of the N=O bond of CNSB

was monotonously reduced with CO_2 pressure (Fig. 8). Namely, the reactivity of the $-NO_2$ group may decrease with CO_2 pressure up to 6 MPa and will not change so much at higher pressures. In contrast, the reactivity of the N=O group may increase with CO_2 pressure. It is likely, therefore, that the hydrogenation of CNSB is more significantly accelerated than that of CNB when dense-phase CO_2 is used. Moreover, the FTIR results indicate that interactions occurred between CPHA and dense-phase CO_2 molecules. These interactions should promote the transformation of CPHA to CAN (step III in Scheme 1), contributing to the improved selectivity to CAN. As a result, CAN was formed with almost 100% selectivity in/under dense-phase CO_2. Therefore, the molecular interactions of CO_2 with the reacting species should be an important factor in determining the product selectivity over Ni/TiO_2.

3.6. Reaction pathways for the hydrogenation of CNB in $scCO_2$ over Ni/TiO_2

The path IV in Scheme 1 occurs on Au/TiO_2, and the step V becomes significant over Pd/Pt/Ni catalysts in the presence of vanadium promoters [2,3,7]. Herein, we discuss the reaction pathways over Ni/TiO_2 in dense-phase CO_2 without the consideration of pathways IV and V. The total yield of all byproducts was <3.5% over the whole conversion range of 9–100% (Fig. 2 and Table 2). Accordingly, the condensation route (steps VI and VII) in Scheme 1 should be negligible, and the hydrogenation of CNB to CAN proceeds likely through the consecutive steps I → II → III. The rate of CAN formation is determined by the slowest reaction rate among steps I, II, and III. The intermediates, detected by GC analysis, included CNSB and trace amounts of CAOB, CAB, and CHAB. These intermediates may be present in the reaction mixture; or they are absent in the reaction mixture but come from the decomposition of CPHA during the GC analysis [42]. Anyway, if the reaction rate of step II or III is the slowest, the amount of these intermediates should increase first and then decrease with the conversion of CNB. Fig. 2 shows that the yield of all byproducts decreased from 3.5% at 9% conversion to <1% at conversion >70%. The yield of CAN was similar to the conversion of CNB over the conversion range of 9–100%. In other words, the rate of CAN formation was almost equal to that of CNB conversion, i.e., the rate of step I. Therefore, in the present case of CNB hydrogenation in dense-phase CO_2 over Ni/TiO_2, the transformation of CNB to CNSB (step I in Scheme 1) seems to be the relatively slow step that determines the rate of CAN formation. The proposed reaction pathways may be related to the molecular interactions of CO_2 with CNB, CNSB, and CPHA. The relative reactivity of these reacting species was changed through interactions with CO_2 as discussed above, and consequently, the relative hydrogenation rates of steps I, II, and III are altered in dense-phase CO_2.

4. Conclusions

The chemoselective hydrogenation of CNB to CAN was achieved over Ni/TiO_2 in $scCO_2$ at 35 °C. Both the accumulation of harmful intermediates and the formation of dechlorinated byproduct were suppressed effectively in $scCO_2$. The selectivity to the desired product, CAN, was >97% over the conversion range of 9–100%. One of the important factors for this improved selectivity to CAN is the interactions of CO_2 with the reacting species, i.e., CNB, CNSB, and CPHA. The nitro group of CNB interacts with CO_2 through its nitrogen and oxygen atoms. The former mode has a dominant effect on the stretch vibration of N–O bond, and the reactivity of CNB is decreased. The nitroso group of CNSB interacts through its oxygen with the carbon of CO_2 and the reactivity of CNSB is increased. CPHA can also interact with $scCO_2$, and the transformation of CPHA to CAN is likely promoted. Probably, the hydrogenation of CNB mainly occurs through the direct hydrogenation route, i.e., CNB → CNSB → CPHA → CAN. The transformation of CNB to CNSB might be the rate-determining step.

The strength of the N–O bond of CNB, the N=O bond of CNSB, and the N–O bond of CPHA is weaker compared with the corresponding bonds of nitrobenzene, nitrosobenzene, and *N*-phenylhydroxylamine, due to the electron-withdrawing effect of Cl substituent. There is no interaction between CO_2 and the nitrogen of N=O group of CNSB, which is different from the modes of CO_2 interaction with nitrosobenzene. The available sites to interact with CO_2 are also less within the CPHA molecule than within the *N*-phenylhydroxylamine one.

Acknowledgments

The authors gratefully acknowledge the financial support from the One Hundred Talent Program of CAS, NSFC 20873139, and KJCX2, YW.H16. This work was also supported by the Japan Society for the Promotion of Science with Grant-in-Aid for Scientific Research (B) 18360378 and by the CAS-JSPS International Joint Project GJHZ05. X. Meng thanks the Global COE (Center of Excellence) fellowship of Hokkaido University.

References

[1] X. Wang, M. Liang, J. Zhang, Y. Wang, Curr. Org. Chem. 11 (2007) 299.
[2] A. Corma, P. Concepcion, P. Serna, Angew. Chem., Int. Ed. 46 (2007) 7266.
[3] P. Baumeister, H.U. Blaser, M. Studer, Catal. Lett. 49 (1997) 219.
[4] H.U. Blaser, A. Schnyder, H. Steiner, F. Rossler, P. Baumeister, in: G. Ertl, H. Knözinger, F. Schüth, J. Weitkamp (Eds.), Handbook of Heterogeneous Catalysis, Wiley-VCH Verlag GmbH & Co. KGaA, Weinheim, Germany, 2008, p. 3291.
[5] F. Cardenas-Lizana, S. Gomez-Quero, M. Keane, Appl. Catal. A 334 (2008) 199.
[6] A. Corma, P. Serna, Science 313 (2006) 332.
[7] M. Studer, S. Neto, H.U. Blaser, Top. Catal. 13 (2000) 205.
[8] N. Mahata, A.F. Cunha, J.J.M. Órfão, J.L. Figueiredo, Catal. Commun. 10 (2009) 1203.
[9] F. Cárdenas-Lizana, S. Gómez-Quero, A. Hugon, L. Delannoy, C. Louis, M. Keane, J. Catal. 262 (2009) 235.
[10] Y. Chen, C. Wang, H. Liu, J. Qiu, X. Bao, Chem. Commun. (2005) 5298.
[11] Y. Chen, J. Qiu, X. Wang, J. Xiu, J. Catal. 242 (2006) 227.
[12] D. He, H. Shi, Y. Wu, B. Xu, Green Chem. 9 (2007) 849.
[13] L. Liu, B. Qiao, Y. Ma, J. Zhang, Y. Deng, Dalton Trans. (2008) 2542.
[14] X. Wang, M. Liang, H. Liu, Y. Wang, J. Mol. Catal. A 273 (2007) 160.
[15] M. Liang, X. Wang, H. Liu, H. Liu, Y. Wang, J. Catal. 255 (2008) 335.
[16] F. Wang, J. Liu, X. Xu, Chem. Commun. (2008) 2040.
[17] B. Coq, A. Tijani, R. Dutartre, F. Figuéras, J. Mol. Catal. 79 (1993) 253.
[18] A. Corma, P. Serna, P. Concepción, J. Calvino, J. Am. Chem. Soc. 130 (2008) 8748.
[19] J. Xiong, J. Chen, J. Zhang, Catal. Commun. 8 (2007) 345.
[20] C. Xiao, H. Wang, X. Mu, Y. Kou, J. Catal. 250 (2007) 25.
[21] C.A. Eckert, B.L. Knutson, P.G. Debenedetti, Nature 383 (1996) 313.
[22] P.G. Jessop, W. Leitner, in: P.G. Jessop, W. Leitner (Eds.), Chemical Synthesis Using Supercritical Fluids, Wiley-VCH, Weinheim, Germany, 1999, p. 9.
[23] A. Baiker, Chem. Rev. 99 (1999) 453.
[24] B.M. Bhanage, M. Arai, Catal. Rev. Sci. Eng. 43 (2001) 315.
[25] J.R. Hyde, P. Licence, D. Carter, M. Poliakoff, Appl. Catal. A 222 (2001) 119.
[26] W. Leitner, Acc. Chem. Res. 35 (2002) 746.
[27] E.J. Beckman, J. Supercrit. Fluid 28 (2004) 121.
[28] B. Subramaniam, M.A. McHugh, Ind. Eng. Chem. Process Des. Dev. 25 (1986) 1.
[29] C.M. Rayner, Org. Process Res. Dev. 11 (2007) 121.
[30] T. Seki, J.D. Grunwaldt, A. Baiker, Ind. Eng. Chem. Res. 47 (2008) 4561.
[31] F. Zhao, S. Fujita, S. Akihara, M. Arai, J. Phys. Chem. A 109 (2005) 4419.
[32] S. Ichikawa, M. Tada, Y. Iwasawa, T. Ikariya, Chem. Commun. (2005) 924.
[33] F. Zhao, R. Zhang, M. Chatterjee, Y. Ikushima, M. Arai, Adv. Synth. Catal. 346 (2004) 661.
[34] F. Zhao, Y. Ikushima, M. Arai, J. Catal. 224 (2004) 479.
[35] C. Xi, H. Cheng, J. Hao, S. Cai, F. Zhao, J. Mol. Catal. A 282 (2008) 80.
[36] M. Mihaylov, E. Ivanova, Y. Hao, K. Hadjiivanov, H. Knözinger, B.C. Gates, J. Phys. Chem. C 112 (2008) 18973.
[37] X. Meng, H. Cheng, Y. Akiyama, Y. Hao, W. Qiao, Y. Yu, F. Zhao, S. Fujita, M. Arai, J. Catal. 264 (2009) 1.
[38] A. Defoin, Synthesis (2004) 706.
[39] O. Kamm, C.S. Marvel, Org. Synth. 4 (1925) 57.
[40] S. Ung, A. Falguières, A. Guy, C. Ferroud, Tetrahedron Lett. 46 (2005) 5913.
[41] G. Bergeret, P. Gallezot, in: G. Ertl, H. Knözinger, F. Schüth, J. Weitkamp (Eds.), Handbook of Heterogeneous Catalysis, Wiley-VCH Verlag GmbH & Co. KGaA, Weinheim, Germany, 2008, p. 738.

[42] S. Galvagno, A. Donato, G. Neri, R. Pietropaolo, Z. Poltarzewski, J. Mol. Catal. 42 (1987) 379.
[43] S. Meijers, V. Ponec, J. Catal. 160 (1996) 1.
[44] Y.K. Agrawal, J. Chem. Eng. Data 22 (1977) 70.
[45] Y. Wu, J. Jiang, Y. Ozaki, J. Phys. Chem. A 106 (2002) 2422.
[46] J.D. Grunwaldt, R. Wandeler, A. Baiker, Catal. Rev. Sci. Eng. 45 (2003) 1.
[47] T. Seki, J.D. Grunwaldt, A. Baiker, J. Phys. Chem. B 113 (2009) 114.
[48] S.G. Kazarian, M.F. Vincent, F.V. Bright, C.L. Liotta, C.A. Eckert, J. Am. Chem. Soc. 118 (1996) 1729.
[49] J.C. Dobrowolski, M.H. Jamróz, J. Mol. Struct. 275 (1992) 211.